The static behavior of RF MEMS capacitive switches in contact

H.M.R. Suy*, R.W. Herfst*, P.G. Steeneken*, J. Stulemeijer** and J.A. Bielen**

* NXP Semiconductors Research, High Tech Campus 37
5656 AE Eindhoven, The Netherlands, hilco.suy@nxp.com
** NXP Semiconductors, Gerstweg 2
6534 AE Nijmegen, The Netherlands

ABSTRACT

A method is presented in which surface topography characterization is combined with the electrical measurement of the contact mechanics under electrostatic loading. Contact characteristics such as the surface separation versus the applied pressure, and the applied pressure versus the contact area, are derived. Based on these results, a contact model is validated. In combination with a compact model of a capacitive switch, this contact model is used to predict the contact behavior of different switch designs.

Keywords: MEMS switches, RF MEMS, contact, contact model, surface roughness

1 INTRODUCTION

Mechanical contact plays a crucial role in MEMS switches, influencing, for example, contact resistance in Ohmic contact switches [1], [2] and reliability (stiction and wear) in general [3], [4]. In this study, we focus on the contact between a membrane and a dielectric in a capacitive switch, and its influence on the capacitance density and slope of the capacitance versus voltage (C-V) curve above pull-in. Depending on the layout of the device, these two parameters affect important switch properties, such as the on-off capacitance ratio, the pull-out voltage, and the capacitance drift in case of dielectric charging. The comprehension of the contact mechanism, and the predictive modeling of such behavior, is thus essential for successful future integration of these devices in, for instance, adaptive antenna matching modules and reconfigurable RF circuits. The goal is to combine surface topography measurements with standard C-V measurements to obtain contact characteristics that can be used to: i) validate contact models more accurately, ii) assist in the contact model parameter extraction, and iii) predict the behavior of other switch designs.

2 METHODS AND RESULTS

Every surface has some degree of roughness. One method to characterize surface topography is Atomic Force Microscopy (AFM), in which a cantilever with a sharp tip is used to scan a surface. Here, the dynamic tapping mode is employed to avoid cantilever stiction. As mentioned in the introduction, the surface topography characterization results (discussed in detail in subsection 2.1) are combined with measurements of the contact mechanics under electrostatic loading (subsection 2.2). These contact mechanics measurements are carried out via C-V measurements on a customized RF setup at a probing frequency of 890 MHz [5]. The combined results of the AFM and C-V measurements are discussed in subsection 2.3 and compared to a contact model.

2.1 Surface Topography Characterization

A Scanning Electron Microscopy (SEM) image of the capacitive switch under study is shown in figure 1. The

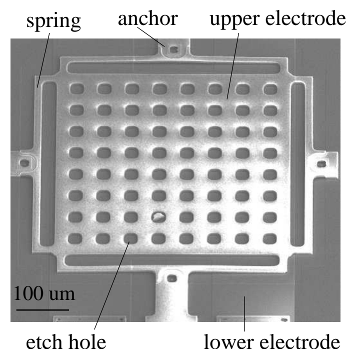

Figure 1: SEM image of the MEMS capacitive switch under study.

switch consists of a perforated upper electrode (membrane) that is suspended by springs over a lower electrode, covered with a dielectric. For various devices, the membrane is removed and flipped so that the bottom is exposed, after which the surface height is measured with AFM on different parts of the membrane. From the AFM data (figure 2), relevant statistical parameters such as the standard deviation, skewness and kurtosis (measure of asymmetry and number of outliers in a statistical distribution, respectively) are calculated, as well as a 2D autocorrelation function. The results (figures 3 and 4) show that the surface height distribution is close to Gaussian, and that no spatial periodic components are present. No dependency on wafer location, switch

design, place on the sample, and number of switching cycles, is observed.

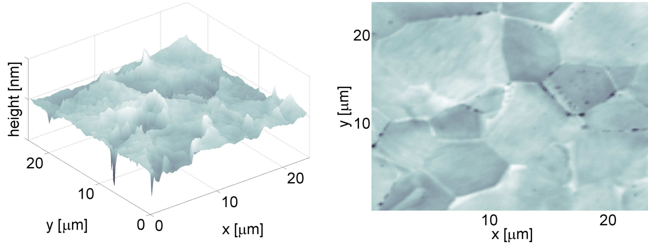

Figure 2: AFM measurement of the bottom of a switch membrane. A planar view is presented on the right, showing the granular structure of the membrane.

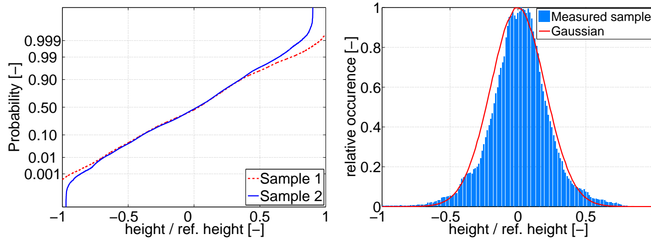

Figure 3: Normal probability plot (left) and histogram (right) of the surface height, normalized to an arbitrary reference height. In the histogram, a comparison is made with an ideal Gaussian distribution, which would produce a straight line in the normal probability plot.

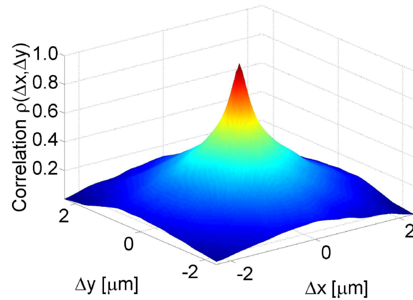

Figure 4: 2D autocorrelation function of the surface height of a sample.

After removal of the membrane, the other contacting surface, the dielectric, is also measured and found to be relatively flat compared to the bottom of the membrane. Because the dielectric material is also much harder than the membrane material, the contact between membrane and dielectric can be regarded as the contact between the membrane and an infinitely hard smooth surface.

2.2 Contact Mechanics Measurement

For seven switches differing in membrane size and spring layout, the C-V curve is measured. The number of switching cycles does not influence the C-V curve, ruling out that plastic deformation occurs. De-embedding is employed to reduce the influence of parasitics. From the de-embedded C-V curve above pull-in, both the applied pressure p_{appl} and the separation g_{eq} between the midplane of the rough membrane and the flat dielectric are estimated. This procedure will be explained using figure 5.

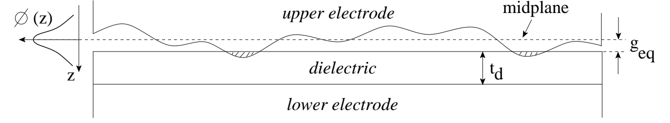

Figure 5: Schematic representation of a rough surface in contact with a flat dielectric.

A rough surface with height distribution $\phi(z)$ is brought into contact with a flat dielectric of thickness t_d, at a midplane distance of g_{eq}. We have seen above that $\phi(z)$ is Gaussian with standard deviation σ:

$$\phi(z) = \frac{1}{\sigma\sqrt{2\pi}} \exp(-z^2/2\sigma^2)\,. \tag{1}$$

The material in contact (shaded, protruding area) is assumed not to influence the distribution $\phi(z)$ [6], [7]. Because the lateral spatial component of the rough surface (correlation length in figure 4) is much larger than the standard deviation σ, fringing field contributions to the capacitance can be neglected. Also, fringing contributions arising from the edges and finite thickness of the membrane are insignificant in closed-state [8], and the closed-state capacitance equals:

$$C(g_{eq}) = \epsilon_0 A \left[\int_{-\infty}^{g_{eq}} \frac{\phi(z)}{g_{eq} - z + t_d/\epsilon_d} dz + \int_{g_{eq}}^{\infty} \frac{\phi(z)}{t_d/\epsilon_d} dz \right], \tag{2}$$

with ϵ_0 the dielectric constant of vacuum (or air), ϵ_d the relative permittivity of the dielectric, and A the nominal membrane area. Expression (2) can be evaluated numerically and compared to the parallel plate approximation of two flat surfaces separated by a gap g_{eq} and dielectric t_d:

$$C_{pp}(g_{eq}) = \frac{\epsilon_0 A}{g_{eq} + t_d/\epsilon_d}\,. \tag{3}$$

The results in figure 6 show that for values of σ around the measured one (σ_{meas}), the capacitance can be approximated by the parallel plate capacitance (solid lines). In practice, elastic contact will remain in the upper regions of separation ($2 < g_{eq}/\sigma < 3$), resulting in a contact area that is only a small fraction ($< 1\%$) of the nominal area, but still sufficient to carry the total load [9], [10]. For this region of interest of g_{eq}/σ, the error between (3) and (2) remains below 5%. This error decreases with t_d/ϵ_d, which here approximately equals 3σ.

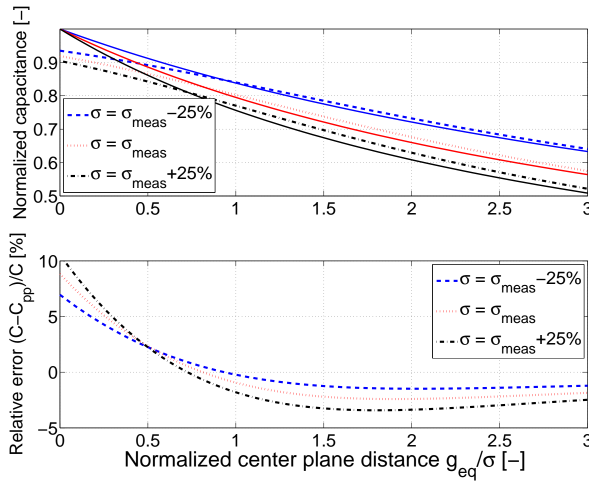

Figure 6: Capacitance of a rough surface C eq. (2) (dashed lines) compared to the parallel plate capacitance C_{pp} eq. (3) (solid lines) for various values of σ.

The surface separation g_{eq} can thus be easily extracted from (3), instead of the more complex (2). Furthermore, the difference in slope dC/dg_{eq} between (2) and (3) for $2 < g_{eq}/\sigma < 3$ is negligible, which means that the electrostatic force can be approximated using (3):

$$F_{el} = \frac{\epsilon_0 A}{2(g_{eq} + t_d/\epsilon_d)^2} V^2 \,, \tag{4}$$

with V the applied voltage. After rewriting, the electrostatic pressure equals:

$$p_{el} = \frac{F_{el}}{A} = \frac{C_{pp}^2 V^2}{2\epsilon_0 A^2} \,. \tag{5}$$

In the voltage region above pull-in, the elastic (spring) forces counteracting the electrostatic force are relatively small and partial release is relatively insignificant, so that the applied contact pressure $p_{appl} \approx p_{el}$.

2.3 Contact Model and Combined Results

In literature, many contact models are described, of which the Greenwood model [9] is widely regarded as the classical work in this field. In this model, the rough surface is regarded as a Gaussian distribution of spherical summits with constant radius. Various adaptations to the Greenwood contact model have been made, for example by Whitehouse and Archard [11] to include varying summit radii. Some other contact models use an exponential force expression [12] or fractal theory [13]. Elaborate overviews of contact models are presented in [10], [14], and [15].

The main drawback of many contact models is the number of required model parameters and/or the unclear parameter extraction method. Therefore, the Mikić model [16] is chosen based on its theoretical background, the availability of closed-form expressions, the low number of parameters and their ease of extraction. The contact model is based on the bearing area method [6], [7], in which an estimate of the contact area A_g is obtained:

$$A_g(g_{eq}) = A \int_{g_{eq}}^{\infty} \phi(z)dz = \frac{A}{2}\mathrm{erfc}\left(\frac{h}{\sqrt{\pi}}\right) . \tag{6}$$

Here, $h = g_{eq}/\sigma$ is the dimensionless separation. The contact force F_c is then given by:

$$F_c = H_E A_g = \frac{E\theta}{\sqrt{2}} A_g \,, \tag{7}$$

with elastic hardness H_E, Young's modulus E and mean absolute slope of the surface roughness θ. The determination of θ is often prone to measurement noise. Therefore, as an alternative, the indentation hardness H is often used as an approximation of H_E. Here, the same method is applied, so that the contact model only has two parameters: the standard deviation σ (measured with AFM) and the indentation hardness H (measured in this research with a Berkovich tip).

The measured separation versus applied pressure characteristic (compliance curve) is shown in figure 7. All

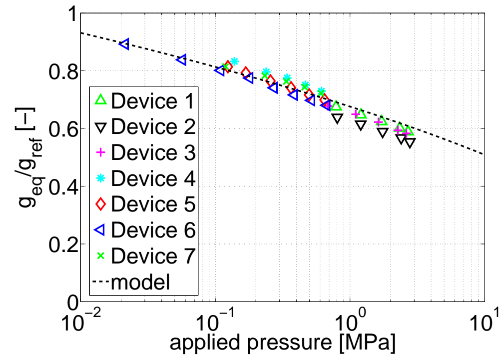

Figure 7: Compliance curve of the separation g_{eq} (normalized to an arbitrary reference gap g_{ref}) versus the logarithm of the applied pressure.

seven devices follow the same trend, independent of membrane size and spring layout, confirming the assumption that elastic forces and partial release can be ignored in this analysis. Furthermore, the separation decreases approximately linearly with the logarithm of the applied pressure. Although already observed for macroscopic rough surfaces in tribology [17], [18], this is the first time that such behavior is shown to hold for MEMS switches. The Mikić model prediction of the compliance curve is also plotted in figure 7, showing good agreement.

Because AFM measurements are relatively time consuming, four out of seven devices on which C-V measurements are carried out and that cover a wide range of applied pressures, are selected. On these four devices,

AFM measurements are performed. The bearing area is taken from the AFM data by measuring the geometrical intersection area of the rough surface (e.g. figure 2) and a horizontal plane at a distance g_{eq} with image processing techniques. In combination with the compliance curve, the applied pressure versus contact area characteristic is then obtained (figure 8). The Mikić model output (6), (7) is also shown. Despite some spread in

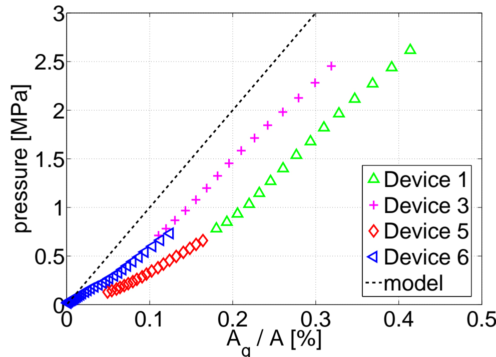

Figure 8: Applied pressure as a function of the bearing area ratio A_g/A.

the measurement results, it can be seen that the applied pressure is approximately linearly dependent on the bearing area ratio, in agreement with Amonton's law of friction [7], [17]. Other sources indicate that a slight deviation from linearity can occur [18], [19]. Here, for the first time, this type of characteristic is evaluated on MEMS structures. The discrepancy between model and measurements in figure 8 can be caused by the samples not being as perfectly Gaussian as the model assumes, and the inaccuracy in the determination of the contact hardness. However, this characteristic can be used to obtain a more accurate estimate of the elastic hardness H_E, which is, as mentioned, difficult to measure.

Finally, the contact model is validated by implementing it in a compact model of the switch [8] and predicting the C-V curve above pull-in for five devices that have designs differing from the seven original ones (figure 9). Both the C-V curve slope and the capacitance density are very well predicted, without the need for fitting.

3 CONCLUSIONS

A method to measure and analyze the static behavior of RF MEMS capacitive switches in contact is demonstrated that combines AFM measurements with standard C-V measurements. Important characteristics that have not been characterized in the field of MEMS before, and that are valuable in the evaluation of contact models, have been analyzed. The presented characteristics are in accordance with the behavior as identified in the field of tribology. The Mikić contact model applied here shows

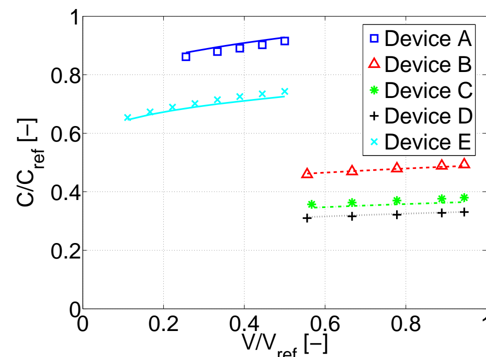

Figure 9: Measured (symbols) and modeled (lines) C-V curves above pull-in for five validation devices, normalized to an arbitrary reference capacitance C_{ref} and voltage V_{ref}.

good agreement with the measurements and is implemented in a compact model of the switch.

ACKNOWLEDGEMENTS

This work was partially supported by the Point-One project MEMSland.

REFERENCES

[1] O. Rezvanian *et al.*, J. Micromech. Microeng. **17**, pp.2006–2015 (2007).
[2] D. Hyman *et al.*, IEEE Trans. on CPT **22**, pp.357–364 (1999).
[3] D.L. Liu *et al.*, Appl. Phys. Lett. **91**, pp.043107-1-3 (2007).
[4] N. Tayebi *et al.*, J. Appl. Phys. **98**, pp.073528-1-13 (2005).
[5] R.W. Herfst *et al.*, IEEE IRPS 2007, pp.417–421.
[6] E.J. Abbott *et al.*, Mechanical Engineering **55**, pp.569–572 (1933).
[7] K.L. Johnson, *Contact Mechanics* (1985).
[8] H.M.R. Suy *et al.*, Nanotech MSM 2007 **3**, pp.65–68.
[9] J.A. Greenwood *et al.*, Proc. Roy. Soc. London **295**, pp.300–319 (1966).
[10] T.R. Thomas (ed.), *Rough Surfaces* (1982).
[11] D.J. Whitehouse *et al.*, Proc. Roy. Soc. London **316**, pp.97–121 (1970).
[12] J.A. Bielen *et al.*, IEEE EuroSime 2007, pp.59–64.
[13] A. Majumdar *et al.*, Journal of Tribology **113**, pp.1–11 (1991).
[14] A. Hariri *et al.*, J. Micromech. Microeng. **16**, pp.1195–1206 (2006).
[15] G. Zavarise *et al.*, Wear **257**, pp.229–245 (2004).
[16] B.B. Mikić *et al.*, Int. J. Heat Mass Transfer **17**, pp.205–214 (1974).
[17] N. Kikuchi *et al.*, *Contact Problems in Elasticity* (1988).
[18] K.L. Woo *et al.*, Wear **58**, pp.331–340 (1980).
[19] I.V. Kragelsky *et al.*, *Friction and Wear* (1965).